Fano effect of a parallel-coupled triple Rashba quantum dot system*

He Ze-Long(贺泽龙)[a)b)], Lü Tian-Quan(吕天全)[a)†], Cui Lian(崔 莲)[a)], Xue Hui-Jie(薛惠杰)[a)c)], Li Lin-Jun(李林军)[a)b)], and Yin Hai-Tao(尹海涛)[c)]

[a)] *Center for Condensed-Matter Science and Technology, Harbin Institute of Technology, Harbin* 150080, *China*

[b)] *Department of Electronic Engineering, Heilongjiang Institute of Technology, Harbin* 150050, *China*

[c)] *School of Physics and Electronic Engineering, Harbin Normal University, Harbin* 150025, *China*

(Received 24 February 2011; revised manuscript received 19 June 2011)

Using the nonequilibrium Keldysh Green's function technique, the Fano effect of a parallel-coupled triple Rashba quantum dot system is investigated. The conductance as a function of electron energy is numerically calculated. Compared with the case of a parallel-coupled double quantum dot system, two additional Fano resonance peaks occur in the conductance spectrum. By adjusting the structural parameters, the two Fano resonance peaks may change into the resonance peaks. In addition, the influence of Rashba spin–orbit interaction on the conductance is studied.

Keywords: nonequilibrium Green's function, Fano effect, quantum dot, electronic transport

PACS: 73.63.–b, 73.23.–b, 05.60.Gg **DOI:** 10.1088/1674-1056/20/11/117303

1. Introduction

Electronic transport through a coupled quantum dot system has been studied by many researchers.[1−7] Coupled quantum dots enables the investigation of various important transport phenomena, such as quantum interference,[8,9] Kondo effects[10−12] and Fano effect[13−17] for its tunable parameters. In recent years, much attention has been paid to the Fano effect.[13−17] The Fano effect, originating from the interference between a discrete state in the quantum dots and a continuum in the lead, is a good probe for phase coherence in mesoscopic devices and shows a typical asymmetric line shape in the conductance spectra.

The Aharonov–Bohm interferometer with double quantum dots has been designed for the quantum information applications, the fundamental studies of quantum molecular effects, and the exploitation of nanospintronic functionalities. In Ref. [18], de Guevara *et al.* found that the conductance in a double-dot interferometer can be separated into one Breit–Wigner resonance centred in the bonding state and one Fano resonance at the antibonding energy. By adjusting the dot-lead coupling strength, the magnetic flux parameter, the positions and the widths of the resonance peaks in the bonding and antibonding states can be manipulated or even interchanged,[19] which may be of importance in device design and quantum computation. In this paper, the Fano effect through a parallel-coupled triple Rashba quantum dot system (see Fig. 1) is investigated. Our formalism is based on the nonequilibrium Green's function proposed by Jauho *et al.*[20] The electron–electron Coulomb interaction, external magnetic flux and Rashba spin-orbit interaction are considered. The change of the conductance with electron energy level and the influence of Rashba spin–orbit interaction on conductance are discussed.

The rest of the present article is organized as follows. Section 2 is devoted to a model Hamiltonian and the formula of the current. Numerical results and analyses are given in Section 3. We draw the main conclusions in Section 4.

2. Model

We consider three single-level quantum dots forming a triple quantum dot system coupled in parallel to two leads as shown in Fig. 1.

*Project supported by the Youth Foundation of Heilongjiang Province, China (Grant No. QC2009C41) and the Heilongjiang Provincial Natural Science Foundation, China (Grant No. F200939).

†Corresponding author. E-mail: ltq@hit.edu.cn

© 2011 Chinese Physical Society and IOP Publishing Ltd

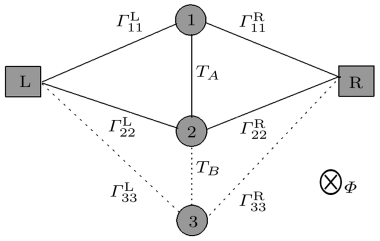


Fig. 1. Schematic setup of the parallel-coupled triple quantum dot system.

The full system can be described by the following Hamiltonian:

$$H_{\rm total} = H_{\rm lead} + H_{\rm dots} + H_{\rm T}, \tag{1}$$

where the first term on the right-hand side, $H_{\rm lead}$, describes the leads in the noninteracting quasiparticle approximation

$$H_{\rm lead} = \sum_{k,\sigma} \sum_{\alpha=L,R} \varepsilon_{k\alpha} C^+_{k\alpha\sigma} C_{k\alpha\sigma}, \tag{2}$$

with $C^+_{k\alpha}(C_{k\alpha})$ being the creation (annihilation) operator of the electron in lead α, and $\varepsilon_{k\alpha}$ denoting the corresponding single particle energy.

The second term of Hamiltonian describes the triple quantum dot system

$$H_{\rm dots} = \sum_{i\sigma} \varepsilon_{i\sigma} d^+_{i\sigma} d_{i\sigma} + \sum_i U_i d^+_{i\uparrow} d_{i\uparrow} d^+_{i\downarrow} d_{i\downarrow} - (T_A d^+_{1\sigma} d_{2\sigma} + T_B d^+_{2\sigma} d_{3\sigma} + {\rm H.C.}), \tag{3}$$

where $d^+_i(d_i)$ represents the creation (annihilation) operator with the energy level $\varepsilon_{i\sigma}$ in the ith quantum dot, $T_A(T_B)$ is the tunneling coupling between the 1st (2nd) and the 2nd (3rd) dots, and U_i expresses the Coulomb repulsion energy in dot i.

The last term on the right-hand side in Eq. (1), $H_{\rm T}$, describes electron tunneling between dots and leads, and takes the form of

$$H_{\rm T} = \sum_i \sum_{k\sigma} \sum_{\alpha={\rm L,R}} (t_{\alpha i\sigma} C^+_{k\alpha\sigma} d_{i\sigma} + {\rm H.C.}), \tag{4}$$

where $t_{\alpha i\sigma}$ describes the dot-lead tunneling coupling, which is assumed to be independent of k. For the sake of simplicity, $t_{\alpha i\sigma}$ are set to be in the following forms, $t_{{\rm L}1\sigma} = |t_{\rm L1}|\,{\rm e}^{{\rm i}\varphi/4}\,{\rm e}^{-{\rm i}\sigma\phi_{\rm R1}/2}$, $t_{{\rm L}2\sigma} = |t_{\rm L2}|\,{\rm e}^{-{\rm i}\sigma\phi_{\rm R2}/2}$, $t_{{\rm L}3\sigma} = |t_{\rm L3}|\,{\rm e}^{-{\rm i}\varphi/4}\,{\rm e}^{-{\rm i}\sigma\phi_{\rm R3}/2}$, $t_{{\rm R}1\sigma} = |t_{\rm R1}|\,{\rm e}^{-{\rm i}\varphi/4}\,{\rm e}^{{\rm i}\sigma\phi_{\rm R1}/2}$, $t_{{\rm R}2\sigma} = |t_{\rm R2}|\,{\rm e}^{\sigma\phi_{\rm R2}/2}$ and $t_{{\rm R}3\sigma} = |t_{\rm R3}|\,{\rm e}^{{\rm i}\varphi/4}\,{\rm e}^{{\rm i}\sigma\phi_{\rm R3}/2}$, where φ is the magnetic flux-induced phase factor. The phase factors $\phi_{\rm R_1}$, $\phi_{\rm R_2}$ and $\phi_{\rm R_3}$ denote the Rashba spin-orbital interactions in dots 1, 2 and 3, respectively. In the following calculations, we define the line-width matrix elements as $\Gamma^\alpha_{ij\sigma} = 2\pi \sum_k t_{\alpha i\sigma} t^*_{\alpha j\sigma} \delta(\varepsilon - \varepsilon_{k\alpha})$, and then the matrix Γ^α_σ can be written as

$$\Gamma^{\rm L}_\sigma = \begin{pmatrix} \Gamma^{\rm L}_1 & \sqrt{\Gamma^{\rm L}_1\Gamma^{\rm L}_2}\,{\rm e}^{\frac{{\rm i}\varphi}{4}}\,{\rm e}^{-\frac{{\rm i}\sigma}{2}(\phi_{\rm R1}-\phi_{\rm R2})} & \sqrt{\Gamma^{\rm L}_1\Gamma^{\rm L}_3}\,{\rm e}^{\frac{{\rm i}\varphi}{2}}\,{\rm e}^{-\frac{{\rm i}\sigma}{2}(\phi_{\rm R1}-\phi_{\rm R3})} \\ \sqrt{\Gamma^{\rm L}_1\Gamma^{\rm L}_2}\,{\rm e}^{-\frac{{\rm i}\varphi}{4}}\,{\rm e}^{\frac{{\rm i}\sigma}{2}(\phi_{\rm R1}-\phi_{\rm R2})} & \Gamma^{\rm L}_2 & \sqrt{\Gamma^{\rm L}_2\Gamma^{\rm L}_3}\,{\rm e}^{\frac{{\rm i}\varphi}{4}}\,{\rm e}^{-\frac{{\rm i}\sigma}{2}(\phi_{\rm R2}-\phi_{\rm R3})} \\ \sqrt{\Gamma^{\rm L}_1\Gamma^{\rm L}_3}\,{\rm e}^{-\frac{{\rm i}\varphi}{2}}\,{\rm e}^{\frac{{\rm i}\sigma}{2}(\phi_{\rm R1}-\phi_{\rm R3})} & \sqrt{\Gamma^{\rm L}_2\Gamma^{\rm L}_3}\,{\rm e}^{-\frac{{\rm i}\varphi}{4}}\,{\rm e}^{\frac{{\rm i}\sigma}{2}(\phi_{\rm R2}-\phi_{\rm R3})} & \Gamma^{\rm L}_3 \end{pmatrix}, \tag{5a}$$

and

$$\Gamma^{\rm R}_\sigma = \begin{pmatrix} \Gamma^{\rm R}_1 & \sqrt{\Gamma^{\rm R}_1\Gamma^{\rm R}_2}\,{\rm e}^{-\frac{{\rm i}\varphi}{4}}\,{\rm e}^{\frac{{\rm i}\sigma}{2}(\phi_{\rm R1}-\phi_{\rm R2})} & \sqrt{\Gamma^{\rm R}_1\Gamma^{\rm R}_3}\,{\rm e}^{-\frac{{\rm i}\varphi}{2}}\,{\rm e}^{\frac{{\rm i}\sigma}{2}(\phi_{\rm R1}-\phi_{\rm R3})} \\ \sqrt{\Gamma^{\rm R}_1\Gamma^{\rm R}_2}\,{\rm e}^{\frac{{\rm i}\varphi}{4}}\,{\rm e}^{-\frac{{\rm i}\sigma}{2}(\phi_{\rm R1}-\phi_{\rm R2})} & \Gamma^{\rm R}_2 & \sqrt{\Gamma^{\rm R}_2\Gamma^{\rm R}_3}\,{\rm e}^{-\frac{{\rm i}\varphi}{4}}\,{\rm e}^{\frac{{\rm i}\sigma}{2}(\phi_{\rm R2}-\phi_{\rm R3})} \\ \sqrt{\Gamma^{\rm R}_1\Gamma^{\rm R}_3}\,{\rm e}^{\frac{{\rm i}\varphi}{2}}\,{\rm e}^{-\frac{{\rm i}\sigma}{2}(\phi_{\rm R1}-\phi_{\rm R3})} & \sqrt{\Gamma^{\rm R}_2\Gamma^{\rm R}_3}\,{\rm e}^{\frac{{\rm i}\varphi}{4}}\,{\rm e}^{-\frac{{\rm i}\sigma}{2}(\phi_{\rm R2}-\phi_{\rm R3})} & \Gamma^{\rm R}_3 \end{pmatrix}, \tag{5b}$$

where Γ^α_i is short for $\Gamma^\alpha_{ii}(i = 1, 2, 3)$.

To describe the non-equilibrium states in the system, we introduce the retarded, advanced and 'lesser' Green functions as follows:

$$G^{\rm r}_{AB}(t,t') = \langle\langle A(t), B(t')\rangle\rangle^{\rm r} = -{\rm i}\theta(t-t')\langle[A(t), B(t')]_+\rangle, \tag{6}$$

$$G^{\rm a}_{AB}(t,t') = \langle\langle A(t), B(t')\rangle\rangle^{\rm a} = {\rm i}\theta(t'-t)\langle[A(t), B(t')]_+\rangle, \tag{7}$$

$$G^{<}_{AB}(t,t') = \langle\langle A(t), B(t')\rangle\rangle^{<} = {\rm i}\langle B(t')A(t)\rangle. \tag{8}$$

Our calculations are limited to the steady state where the Green functions depend only on the variable $\Delta t = t - t'$. By Fourier transforming with respect to variable $t - t'$ in $\langle\langle A(t-t'), B(0)\rangle\rangle$, we can obtain $\langle\langle A, B\rangle\rangle_\omega$. In the present investigations, the knowledge of the Green functions $\langle\langle d_i, d^+_i\rangle\rangle_\omega$ $(i = 1, 2, 3)$ enables us to determine all the transport characteristics of the system. In order to calculate them, we use both the Dyson equation and the equation of motion for each Green's function. By employing the Hartree–Fock approximation to truncate the higher-order Green's function, the retarded (advanced) one can be written as

$$G_\sigma^{\rm r}(\varepsilon)=(G_\sigma^{\rm a}(\varepsilon))^{+}=\begin{pmatrix} S_1+\dfrac{\rm i}{2}(\Gamma_{11}^{\rm L}+\Gamma_{11}^{\rm R}) & T_A+\dfrac{\rm i}{2}(\Gamma_{12}^{\rm L}+\Gamma_{12}^{\rm R}) & \dfrac{\rm i}{2}(\Gamma_{13}^{\rm L}+\Gamma_{13}^{\rm R}) \\ T_A+\dfrac{\rm i}{2}(\Gamma_{21}^{\rm L}+\Gamma_{21}^{\rm R}) & S_2+\dfrac{\rm i}{2}(\Gamma_{22}^{\rm L}+\Gamma_{22}^{\rm R}) & T_B+\dfrac{\rm i}{2}(\Gamma_{23}^{\rm L}+\Gamma_{23}^{\rm R}) \\ \dfrac{\rm i}{2}(\Gamma_{31}^{\rm L}+\Gamma_{31}^{\rm R}) & T_B+\dfrac{\rm i}{2}(\Gamma_{32}^{\rm L}+\Gamma_{32}^{\rm R}) & S_3+\dfrac{\rm i}{2}(\Gamma_{33}^{\rm L}+\Gamma_{33}^{\rm R}) \end{pmatrix}^{-1}, \tag{9}$$

where

$$S_j=\frac{(\varepsilon-\varepsilon_{j\sigma})(\varepsilon-\varepsilon_{j\sigma}-U_j)}{\varepsilon-\varepsilon_{j\sigma}-U_j+U_j\langle n_{j\bar\sigma}\rangle}$$

with $\langle n_{j\bar\sigma}\rangle$ being the average occupation number that needs to be calculated by using the self-consistent

$$\langle n_{j\bar\sigma}\rangle=-{\rm i}\int\frac{{\rm d}\varepsilon}{2\pi}G^{<}_{j\bar\sigma,j\bar\sigma}(\varepsilon).$$

The formula of the currents can be derived as[20]

$$J_\sigma=\frac{e}{\hbar}\int\frac{{\rm d}\varepsilon}{2\pi}\left[f_{\rm L}(\varepsilon)-f_{\rm R}(\varepsilon)\right]{\rm Tr}\times\left[G_\sigma^{\rm a}(\varepsilon)\Gamma_\sigma^{\rm R}G_\sigma^{\rm r}(\varepsilon)\Gamma_\sigma^{\rm L}\right], \tag{10}$$

where $f_\alpha(\omega)=\{1+\exp\left[(\varepsilon-u_\alpha)/k_{\rm B}T\right]\}^{-1}$ is the Fermi distribution function.

The conductance at zero temperature reads

$$G_\sigma(\varepsilon_{\rm F})=\frac{e^2}{\hbar}{\rm Tr}\left[G_\sigma^{\rm a}(\varepsilon)\Gamma_\sigma^{\rm R}G_\sigma^{\rm r}(\varepsilon)\Gamma_\sigma^{\rm L}\right]\big|_{\varepsilon=\varepsilon_{\rm F}}, \tag{11}$$

where $\varepsilon_{\rm F}$ is Fermi level.

3. Numerical results

Using the formulae obtained above, one can numerically calculate the basic transport characteristics of the system. In the following numerical analysis, the levels of the dots are identical ($\varepsilon_{1\sigma}=\varepsilon_{2\sigma}=\varepsilon_{3\sigma}=\varepsilon_0$) and the intradot Coulomb interactions are also taken to be the same ($U_1=U_2=U_3=U$). For simplicity, assume that $\phi_{\rm R_2}=\phi_{\rm R_3}$, then $\Gamma_\sigma^{\rm L,R}$ will depend only on $\phi_{\rm R_{12}}=\phi_{\rm R_{13}}=\phi_{\rm R_1}-\phi_{\rm R_{2(3)}}=\phi_{\rm R}$, which is the difference between $\phi_{\rm R_1}$ and $\phi_{\rm R_2}(\phi_{\rm R_3})$. In addition, we presume that $\Gamma_1^\alpha=\Gamma_2^\alpha=\Gamma(\alpha\in{\rm L,R})$, and take Γ as energy units in the following discussion.

For the parallel-coupled double quantum dot (DQD) system, once one quantum dot impurity couples with the system, the influence of the coupling strength between the quantum dot impurity and the system on the conductance should be studied. Here, the quantum dot 3 can couple with one of the parallel-coupled DQDs and also couple with two leads.

We first consider the cases of the conductance versus electron energy for several values of T_B, when the quantum dot 3 is decoupled from the leads. Electron–electron interaction (assume $U=4$), the magnetic flux (assume $\varphi=0$), and the Rashba spin-orbital interaction (assume $\phi_{\rm R}=\pi/4$) are considered. Figures 2(a)–2(d) show that the conductance spectrum is divided into two groups of resonant peaks, which is due to the coulomb interaction in the quantum dot. At the same time, one can find clearly that the trends of two groups of the resonant peaks are similar and the widths of the conductance peaks located at Coulomb counterparts are narrower. For comparison, the solid line in Fig. 2(a) represents the conductance spectrum of the parallel-coupled DQD system. Here, we consider the Rashba interaction in the quantum dots, which can induce a spin-dependent phase factor. By the action of this phase factor, the transport through dot 1 and dot 2 will provide one nonresonant channel and one resonant tunnel, respectively, which leads to the Fano resonance. As shown by the solid line in Fig. 2(a), the conductance spectrum is composed of two Breit–Wigner and two Fano resonances, centred at bonding energy (ε_0-T_A), antibonding energy (ε_0+T_A) and their Coulomb counterparts, respectively. The results are in good agreement with those obtained in Ref. [14]. When the coupling strength between quantum dot 3 and dot 2 is small enough, i.e., $T_B=0.01$ (the dashed line in Fig. 2(a)), the conductance spectrum shows mainly the transport properties of the parallel-coupled DQD system. An interesting phenomenon is that for the dashed line in Fig. 2(a), two sharp resonance peaks appear at the energy levels $\varepsilon=\varepsilon_0$ and $\varepsilon=\varepsilon_0+U$, respectively. One can see clearly that the solid and dashed curves are consistent with each other except for the two sharp resonance peaks. It means that the influence of the weak coupling between the quantum dot 3 and dot 2 on the conductance through the parallel-coupled DQD system is very small. One can take the weak coupling between the quantum dot 3 and dot 2 as feeble perturbation. With the increase of the coupling strength T_B, the two additional Fano line shapes appear with the narrowing of the Breit–Wigner linewidths (see Figs. 2(b)–2(c)). For the sufficiently large T_B, two additional Fano resonance peaks

change into the resonance peaks (see Fig. 2(d)). Moreover, the positions of the conductance peaks corresponding to the bonding, antibonding energies and their Coulomb counterparts are modulated due to the coupling of the quantum dot 3 to 2. It is obvious that as T_B becomes big, the distance between two resonance peaks corresponding to the bonding and the antibonding energies increases, so does the distance for their Coulomb counterparts. In addition, for the two Fano anti-resonance peaks located at the antibonding energy and the corresponding Coulomb counterpart, one can find that the positions of the anti-resonance point step up and the two Fano resonance peaks also evolve into resonance peaks gently as T_B increases. As shown in Fig. 2(d), six resonance peaks appear in the conductance spectrum. We consider that the reason for the appearance of these phenomena above is that when the coupling strength T_B is doughty enough, the quantum dot 3 and dot 2 form a new quantum state, which affects the quantum interference of the electron waves passing through the parallel-coupled DQD system. Therefore, two Fano anti-resonance points disappear. This leads to the transition from four Fano peaks to four resonance peaks.

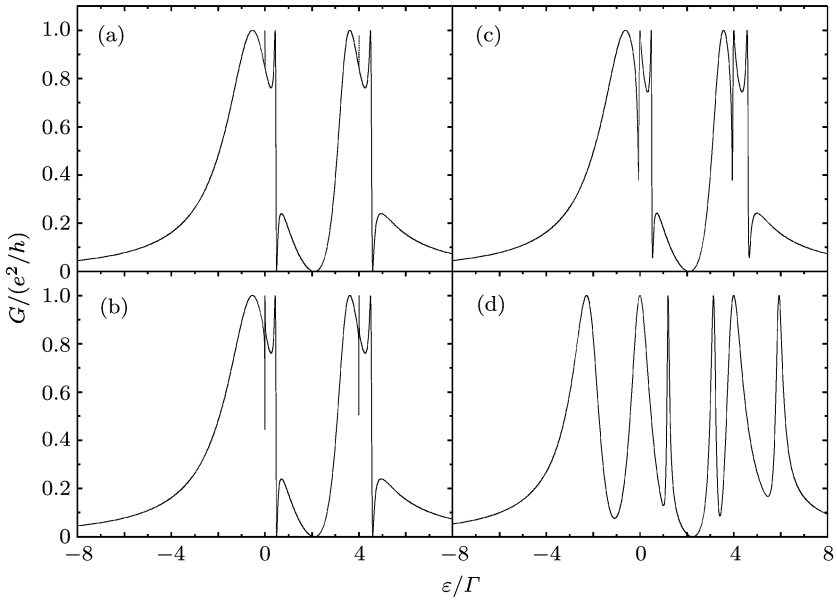


Fig. 2. Conductances versus electron energy for several values of T_B, with parameters being $U = 4$, $T_A = 1$, $\varphi = 0$, $\phi_{\rm R} = \pi/4, \varepsilon_0 = 0$ and $\Gamma_{33}^{\rm L,R} = 0.0$. (a) $T_B = 0.0$ (solid line), $T_B = 0.01$ (dashed line); (b) $T_B = 0.1$; (c) $T_B = 0.5$; (d) $T_B = 3.0$.

The density of states is another physical quantity underlying these transport properties and provides a clear physical picture. The total density of states is defined as $\rho(\varepsilon) = \sum_{i=1}^{3} \rho_i(\varepsilon) = -(1/\pi) \sum_{i=1}^{3} {\rm Im} G_{ii}^{\rm r}(\varepsilon)$. Figure 3 shows the total density of states $\rho(\varepsilon)$ with the same parameters in Fig. 2. The solid line in Fig. 3(a) shows $\rho(\varepsilon)$ of the parallel-coupled DQD system. Two Lorentzian peaks and two peaks with finite widths are found. The dashed line corresponds to $T_B = 0.01$ and shows two δ function types at $\varepsilon = \varepsilon_0$ and $\varepsilon = \varepsilon_0 + U$, respectively. Comparing this feature of density of states with the linear conductance shown by the dashed line in Fig. 2(a), the appearance of two δ function types indicates the formation of two additional sharp resonance peaks. When T_B increases from 0.1 to 3.0, the widths of two δ function types broaden little by little. It is consistent with the conductance spectrum, in which two Fano resonance peaks turn into familiar resonance peaks. Six resonances with finite widths and heights presented in Fig. 3(d) correspond to the six resonance peaks shown in Fig. 2(d).

Next, we consider the cases of the conductance versus electron energy for several values of the coupling strength between the quantum dot 3 and the leads, when the quantum dot 3 decouples with dot 2. For comparison, the solid curve in Fig. 4(a) still represents the conductance spectrum of the parallel-coupled DQD system. As dot 3 weakly couples with the leads, i.e., $\Gamma_3^{\rm L,R} = 0.01$, the dashed line in Fig. 4(a) denote two new Fano resonance peaks appearing at the energy levels $\varepsilon = \varepsilon_0$ and $\varepsilon = \varepsilon_0 + U$, respectively. The others parts are the same as the conductance spectrum through parallel-coupled DQD. This

is because the influence of the coupling strength between the quantum dot 3 and the leads on the transport through parallel-coupled DQD is tiny for a small coupling $\Gamma_3^{\mathrm{L,R}}$. When the coupling strength between dot 3 and the leads is assumed to be $\Gamma_3^{\mathrm{L,R}} = 0.1$, the widths of the two new Fano resonance peaks broaden. As $\Gamma_3^{\mathrm{L,R}}$ further becomes large as shown in Figs. 4(c) and 4(d), two new Fano resonance peaks evolve into familiar resonance peaks gradually. In addition, it can be seen that the positions of two Breit–Wigner and two Fano anti-resonance peaks located at the bonding energy, the antibonding energy and the corresponding Coulomb counterpart always keep unchanged no matter how $\Gamma_3^{\mathrm{L,R}}$ changes. The reason is that the branch for the lead L-dot 3-lead R is an isolated path without coupling the quantum dot 3 to dot 2. Therefore, the intrinsic properties of the parallel-coupled DQD system are reserved.

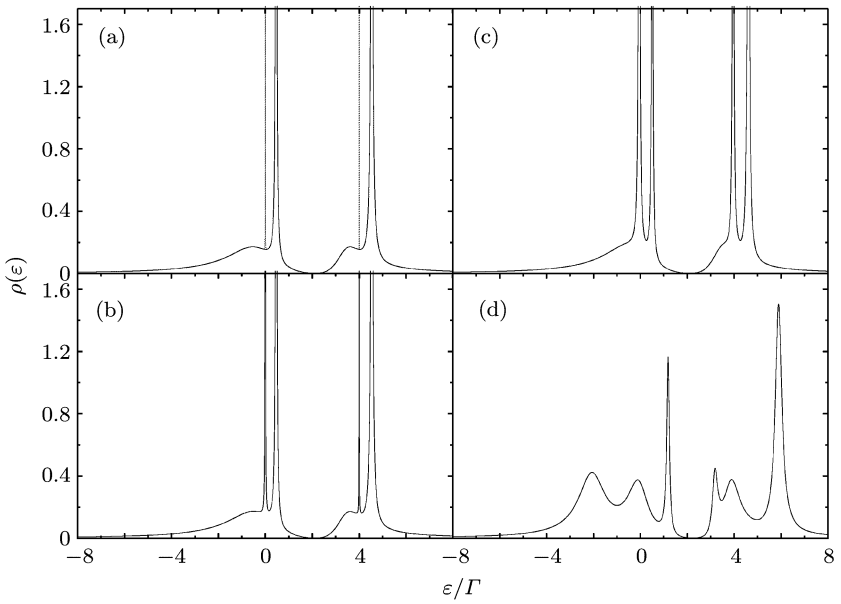


Fig. 3. Densities of state versus the electron energy for several values of T_B. The same parameters are chosen as those in Fig. 2. (a) $T_B = 0.0$ (solid line), $T_B = 0.01$ (dashed line); (b) $T_B = 0.1$; (c) $T_B = 0.5$; (d) $T_B = 3.0$.

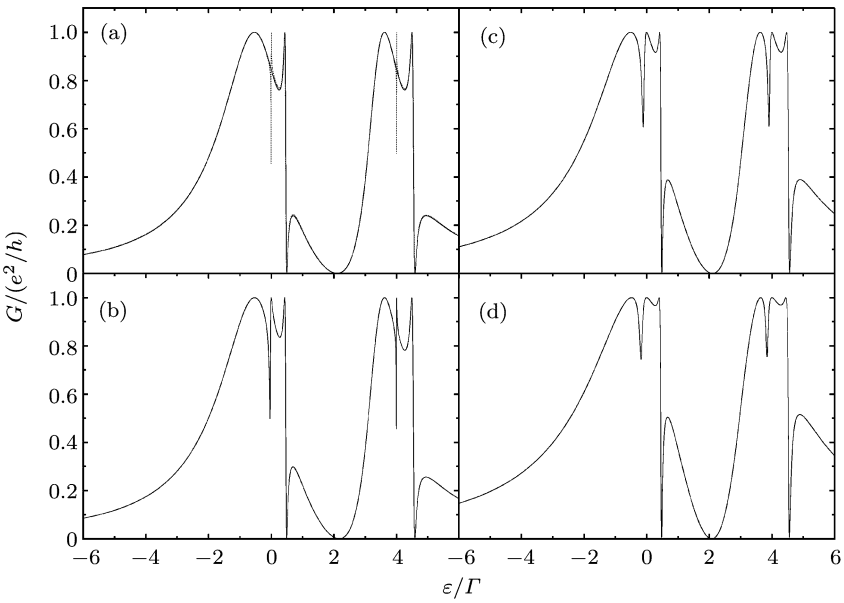


Fig. 4. Conductances versus electron energy for several values of $\Gamma_{33}^{\mathrm{L,R}}$, with parameters being $U = 4$, $T_A = 1$, $\varphi = 0$, $\phi_{\mathrm{R}} = \pi/4$, $\varepsilon_0 = 0$ and $T_B = 0.0$. (a) $\Gamma_{33} = 0.0$ (solid line), $\Gamma_{33} = 0.01$ (dashed line); (b) $\Gamma_{33} = 0.1$; (c) $\Gamma_{33} = 0.5$; (d) $\Gamma_{33} = 1.0$.

Figure 5 shows the total density of states $\rho(\varepsilon)$ with the same parameters as those in Fig. 4. As shown by the dashed line in Fig. 5(a), there are two ultranarrow peaks appearing at $\varepsilon = \varepsilon_0$ and $\varepsilon = \varepsilon_0 + U$, respectively.

Two ultranarrow peaks correspond to two new Fano resonance peaks of the dashed line in Fig. 4(a). With the increase of $\Gamma_{33}^{\mathrm{L,R}}$, the enlarging of the width for two ultranarrow peaks implies that two new Fano resonance peaks in the conductance spectrum become familiar resonance peaks little by little.

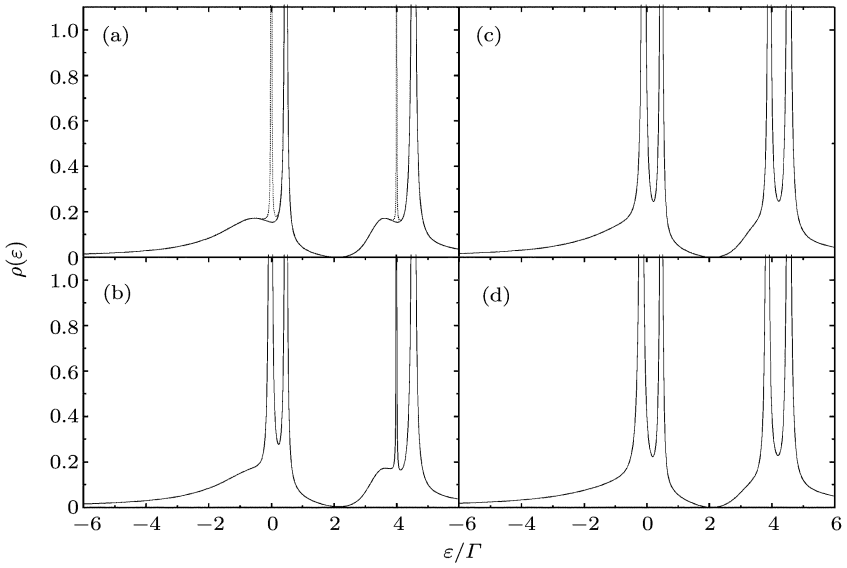


Fig. 5. Densities of state versus electron energy for several values of $\Gamma_{33}^{\mathrm{L,R}}$. The same parameters are chosen as those in Fig. 4. (a) $\Gamma_{33} = 0.0$ (solid line), $\Gamma_{33} = 0.01$ (dashed line); (b) $\Gamma_{33} = 0.1$; (c) $\Gamma_{33} = 0.5$; (d) $\Gamma_{33} = 1.0$.

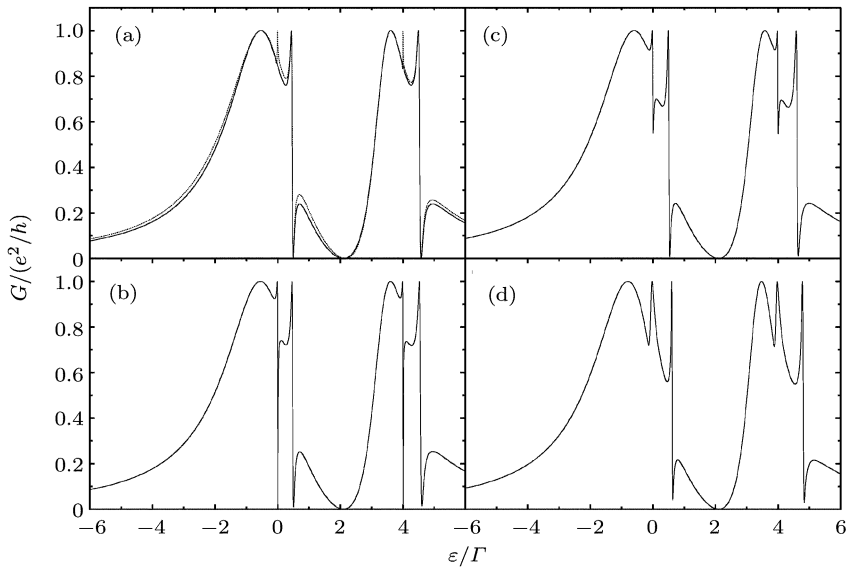


Fig. 6. Conductances versus electron energy for several values of T_B, with parameters being $U = 4$, $T_A = 1$, $\varphi = 0$, $\phi_{\mathrm{R}} = \pi/4$ and $\varepsilon_0 = 0$. (a) $\Gamma_{33} = 0.0$, $T_B = 0.0$ (solid line), $\Gamma_{33} = 0.1$, $T_B = 0.1$ (dashed line); (b) $\Gamma_{33} = 0.1$, $T_B = 0.3$; (c) $\Gamma_{33} = 0.1$, $T_B = 0.5$; (d) $\Gamma_{33} = 0.1$, $T_B = 1.0$.

We also calculate the conductances each as a function of the electron energy for several values of T_B, when the quantum dot 3 weakly couples with the leads ($\Gamma_{33}^{\mathrm{L,R}} = 0.1$). The solid line in Fig. 6(a) still represents the conductance spectrum of the parallel-coupled DQD system. As dot 3 weakly couples with dot 2, i.e., $T_B = 0.1$ (the dashed line in Fig. 6(a)), two sharp resonance peaks appear at the energy levels $\varepsilon = \varepsilon_0$ and $\varepsilon = \varepsilon_0 + U$, respectively. However, the solid and dashed curves in Fig. 6(a) are not entirely consistent with each other. We consider that the branch for the lead L-dot 3-lead R is no longer an isolated path when the dot 3 couples with the dot 2 and the leads, simultaneously. The interference of the electron waves passing through the system becomes more complicated. Hence, the transport properties of the parallel-coupled DQD system are perturbed. When $T_B = 0.3$, the two additional resonance peaks pre-

sented in Fig. 6(a) become two Fano resonance peaks, which seem like Fano antiresonance peaks. When $T_B = 0.5$, two Fano resonance peaks become small. If dot 3 doughtily couples with dot 2, i.e., $T_B = 1.0$, two Fano resonance peaks change into familiar resonance peaks. These behaviours can be understood from the corresponding density of states.

Figure 7 shows the total density of states $\rho(\varepsilon)$ with the same parameters as those in Fig. 6. As shown by the dashed line in Fig. 7(a), there are also two peaks with very narrow widths appearing at $\varepsilon = \varepsilon_0$ and $\varepsilon = \varepsilon_0 + U$, respectively. The two narrow peaks correspond to two sharp resonance peaks in the dashed line in Fig. 6(a). With the increase of T_B, as shown in Figs. 7(b) and 7(c), the line shape of the peak located at $\varepsilon = \varepsilon_0$ resembles that located at the antibonding energy. This coincides with the appearance of the additional Fano resonance peak in the conductance spectrum. As $T_B = 1.0$, the widths of the two peaks corresponding to the energy levels $\varepsilon = \varepsilon_0$ and $\varepsilon = \varepsilon_0 + U$ broaden, which indicates that the two additional Fano resonance peaks in the conductance spectrum turn into familiar resonance peaks.

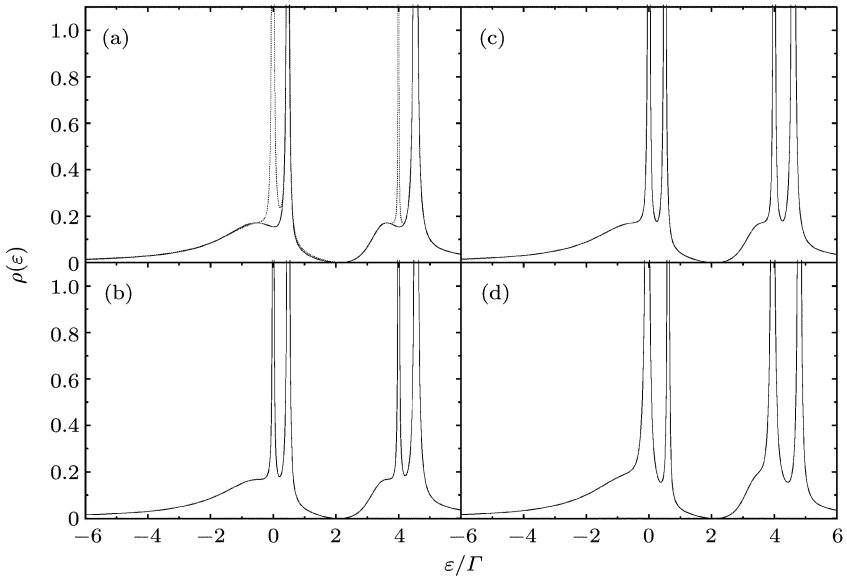


Fig. 7. Densities of state versus electron energy for several values of T_B. The parameters are chosen as those in Fig. 6. (a) $\Gamma_{33} = 0.0$, $T_B = 0.0$ (solid line), $\Gamma_{33} = 0.1$, $T_B = 0.1$ (dashed line); (b) $\Gamma_{33} = 0.1$, $T_B = 0.3$; (c) $\Gamma_{33} = 0.1$, $T_B = 0.5$; (d) $\Gamma_{33} = 0.1$, $T_B = 1.0$.

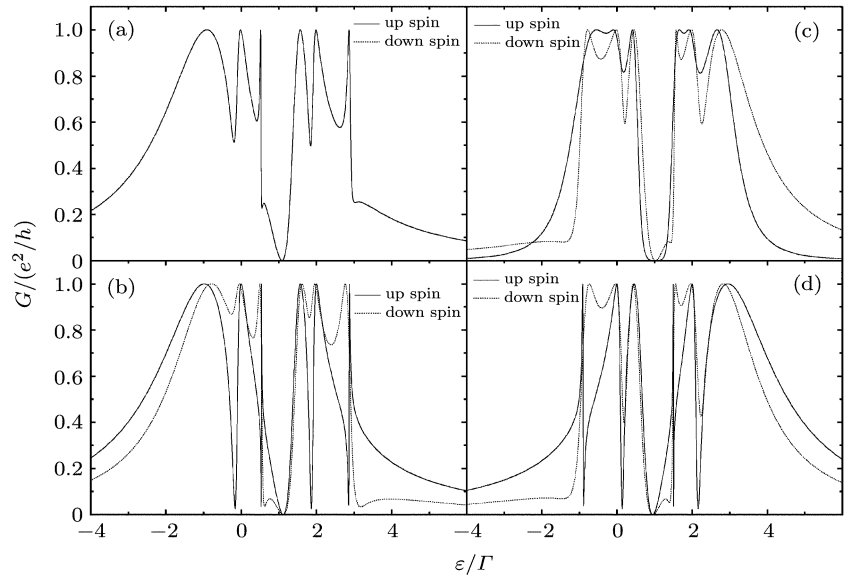


Fig. 8. Conductances versus electron energy for several values of $\varphi_{\rm R}$ with parameters being $U = 2$, $T_A = T_B = 1.0$, $\varphi = \pi/2$, $\varepsilon_0 = 0$ and $\Gamma_3^{\rm L,R} = 0.01$. (a) $\phi_{\rm R} = 0$; (b) $\phi_{\rm R} = \pi/4$; (c) $\phi_{\rm R} = 5\pi/4$; (d) $\phi_{\rm R} = 9\pi/4$.

Finally, the influence of Rashba spin-orbit interaction on the conductance is discussed. The correlative parameters are given by $U = 2$, $T_A = T_B = 1.0$, $\varphi = \pi/2$, $\varepsilon_0 = 0$ and $\Gamma_3^{\mathrm{L,R}} = 0.01$. The peak shape of each spin is sensitive to the ϕ_{R}. As observed from Fig. 8, the main characteristics of the spin polarized conductance can be summarized as follows: 1) in Figs. 8(a)–8(d), one can clearly see that the conductance spectrum is also divided into two groups by an antiresonance point, which is caused by the coulomb interaction in the quantum dot. It is noticeable that for the conductance of the spin up component, an insulating band forms around the energy level $\varepsilon = 1.0$ when $\phi_{\mathrm{R}} = 5\pi/4$; 2) when $\phi_{\mathrm{R}} = 0$, the spin-dependent phase factor satisfies the relation $\phi_\uparrow = \phi_\downarrow$, so that the conductance is spin-independent as shown in Fig. 8(a); 3) when $\phi_{\mathrm{R}} \neq 0$, Figs. 8(b)–8(d) show that the Fano resonance for each spin component is clearly manifested by the asymmetric peak in the conductance spectrum. That is to say, the conductance is spin polarized; 4) for the conductance of spin up component, Fig. 8(b) shows that two Breit–Wigner resonances and four Fano resonances occur in the conductance spectrum. A flip effect can be seen by comparing Fig. 8(b) with Fig. 8(d). It is indicated that the role of the quantum states can be interchanged by controlling the extra phase ϕ_{R}.

4. Conclusion

We investigate nonequilibrium quantum transport through the parallel-coupled triple Rashba quantum dot system under dc bias voltage. The conductance $G(\varepsilon)$ as a function of electron energy ε is analysed. Some significant results are obtained as follows: 1) two additional Fano resonance peaks occur in the conductance spectrum when the quantum dot 3 couples with two leads or one of the parallel-coupled DQDs; 2) two new Fano resonance peaks can also be observed in the conductance spectrum when the dot 3 couples with the leads and dot 2, synchronously, which seems like Fano antiresonance peaks for special value of the coupling strength between the quantum dot 3 and dot 2; 3) the Rashba spin–orbit interaction plays an essential role in spin transport through the system; 4) the role of the quantum states can be interchanged by controlling the extra phase ϕ_{R}. These results are expected to be useful in device design and quantum computation in future.

References

[1] Zhao H K 1997 *Phys. Lett.* A **226** 105

[2] van der Wiel W G, de Franceschi S, Elzerman J M, Fujisawa T, Tarucha S and Kouwenhoven L P 2002 *Rev. Mod. Phys.* **75** 1

[3] Sánchez D and López R 2005 *Phys. Rev.* B **71** 035315

[4] Ye S J, He Z L and Li H 2009 *Phys. Scr.* **79** 035702

[5] He Z L, Lü T Q, Li H and Yin H T 2006 *Phys. Lett.* A **360** 199

[6] Gong W J, Zheng Y S, Liu Y, Kariuki F N and Lü T Q 2008 *Phys. Lett.* A **372** 2934

[7] Wang R, Kong L M, Zhou Y Q, Zhang C X and Xing Z Y 2010 *Chin. Phys.* B **19** 127202

[8] Donarini A, Begemann G and Grifoni M 2010 *Phys. Rev.* B **82** 125451

[9] Hatef A and Singh M R 2010 *Phys. Rev.* A **81** 063816

[10] Malecki J and Affleck I 2010 *Phys. Rev.* B **82** 165426

[11] Sun Q F and Guo H 2001 *Phys. Rev.* B **64** 153306

[12] Žitko R 2010 *Phys. Rev.* B **81** 115316

[13] Goker A 2010 *Phys. Status Solidi* B **247** 129

[14] Yin H T, Lü T Q, Sun P N, Liu X J and Xue H J 2009 *Phys. Lett.* A **373** 3085

[15] Hou T, Wu S Q, Bi A H, Yang F B, Chen J F and Fan M 2009 *Chin. Phys.* B **18** 783

[16] Lu H Z, Lü R and Zhu B F 2006 *Physica* E **34** 538

[17] Chi F and Zheng J 2008 *Appl. Phys. Lett.* **92** 062106

[18] de Guevara M L L, Claro F and Orellana P A 2003 *Phys. Rev.* B **67** 195335

[19] Lu H Z, Lü R and Zhu B F 2005 *Phys. Rev.* B **71** 235320

[20] Jauho A P, Wingreen N S and Meir Y 1994 *Phys. Rev.* B **50** 5528